

Nanoscale Bubble Dynamics Induced by Damage of Graphene Liquid Cells

Hirokawa, Sota

Department of Aeronautics and Astronautics, Kyushu University

Teshima, Hideaki

Department of Aeronautics and Astronautics, Kyushu University

Solís-Fernández, Pablo

Global Innovation Center, Kyushu University

Ago, Hiroki

Global Innovation Center, Kyushu University

他

<https://hdl.handle.net/2324/4793618>

出版情報 : ACS OMEGA. 5 (19), pp.11180-11185, 2020-05-19. American Chemical Society

バージョン :

権利関係 : This is an open access article published under an ACS AuthorChoice License, which permits copying and redistribution of the article or any adaptations for non-commercial purposes.



Nanoscale Bubble Dynamics Induced by Damage of Graphene Liquid Cells

Sota Hirokawa, Hideaki Teshima, Pablo Solís-Fernández, Hiroki Ago, Yoko Tomo, Qin-Yi Li, and Koji Takahashi*



Cite This: *ACS Omega* 2020, 5, 11180–11185



Read Online

ACCESS |



Metrics & More

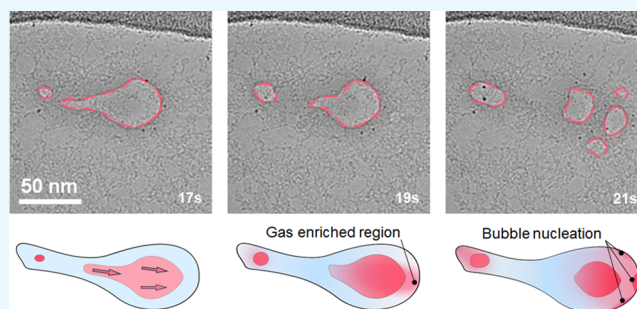


Article Recommendations



Supporting Information

ABSTRACT: Graphene liquid cells provide the highest possible spatial resolution for liquid-phase transmission electron microscopy. Here, in graphene liquid cells (GLCs), we studied the nanoscale dynamics of bubbles induced by controllable damage in graphene. The extent of damage depended on the electron dose rate and the presence of bubbles in the cell. After graphene was damaged, air leaked from the bubbles into the water. We also observed the unexpected directional nucleation of new bubbles, which is beyond the explanation of conventional diffusion theory. We attributed this to the effect of nanoscale confinement. These findings provide new insights into complex fluid phenomena under nanoscale confinement.



INTRODUCTION

With the rapid development of nanostructured materials, such as carbon nanotubes and nanoporous materials, the behavior of water confined in nanoscale spaces has attracted increasing attention.^{1–4} Previous research has revealed the unique properties of nanoscale-confined water, such as a large slip length^{5–10} and an unusual increase in the freezing point of water.^{11–15} This anomalous behavior of nanoscale-confined water expands the possibilities for new and high-efficiency applications of fluidic devices.² To promote the development of such devices, a detailed understanding of the nature of nanoscale-confined water is needed. However, our knowledge is limited owing to the lack of effective experimental techniques.

The atomic-scale spatial resolution and subsecond temporal resolution of transmission electron microscopy (TEM) enable us to observe details of fluidic phenomena in nanoscale spaces.¹⁶ Recently, graphene liquid cells (GLCs) have been developed to achieve higher-resolution liquid-phase observations. The atomic thickness, flexibility, and impermeability to water and gas make graphene an ideal material for liquid cells. However, bubbles often exist in the liquid cell, probably owing to the low pressure in the TEM chamber. Shin et al. first reported the unique dynamics of nanobubbles confined in GLCs.¹⁷ They determined the critical radius of stable nanobubbles and demonstrated nanobubble behavior, including vanishing, Ostwald-ripening, and coalescing. Other nanobubble research using GLCs has focused on the deformation and growth mechanism of bubbles generated by the radiolysis of water.^{18,19} However, the electron beam of TEM is

deleterious not only to the confined liquid but also to graphene. This has remained a key obstacle for long-time observation using GLCs.

Herein, we present the dynamic behavior of nanoscale-confined bubbles and their contribution to the damage of a GLC. First, we investigated the electron-beam damage of GLCs using different TEMs. Then, we introduced damage to graphene to trigger the dynamic behavior of bubbles. The bubbles started shrinking after GLC breakage, and unexpected directional nucleation was observed.

EXPERIMENTAL METHODS

Our GLC was fabricated from bilayer graphene that was synthesized on Cu/Ni by chemical vapor deposition. Detailed methods of our graphene synthesis are given in the reference article.²⁰ A TEM grid (R1.2/1.3 Au 200 mesh, Quantifoil Micro Tools GmbH, Jena, Germany) was placed directly on the graphene and Cu/Ni, whereupon the Cu/Ni–graphene–TEM grid system was immersed in an etching solution to remove the Cu/Ni substrate. The resulting graphene TEM grid was removed from the solution and left in a clean room for 2 h to dry. After drying, approximately 0.5 μ L of air-saturated pure water was dropped on the graphene side of the TEM grid,

Received: March 18, 2020

Accepted: April 24, 2020

Published: May 5, 2020



whereupon another graphene TEM grid was gently placed on top of the water bead to create a sandwich structure with water trapped between the two graphene sheets. When the two graphene sheets came into contact, the water was broken up into many small water pockets. The upper and lower graphene sheets were firmly stacked via the strong van der Waals force, which effectively prevented water from leaking out into the ultrahigh vacuum environment of the TEM chamber. For TEM imaging, we used JEM-2100Plus operating at an electron energy of 200 keV (JEOL Ltd., Tokyo, Japan). The CCD camera equipped in JEM-2100Plus is the Rio16 camera (Gatan, Pleasanton). We also used JEM-ARM200F and JEM-ARM200CF at 200 keV and 60 keV (JEOL Ltd., Tokyo, Japan) with the OneView camera (Gatan, Pleasanton). The dose rate of the thermion gun is 2–3 orders of magnitude lower than the field-emission (FE) gun.

RESULTS AND DISCUSSION

The TEM image in Figure 1 confirms that our sample had many water pockets in the GLC, more than half of which

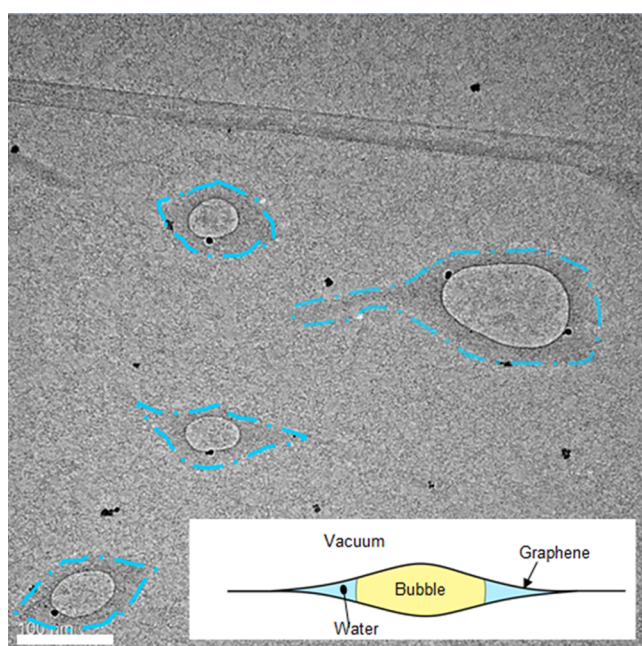


Figure 1. TEM image of water pockets with bubbles. The dashed-dotted lines outline the water pockets. The black dots are assumed to be undissolved Cu/Ni. The scale bar indicates 100 nm. Inset: schematic illustration of the cross section of a water pocket. The original image is shown in Figure S2.

contained bubbles (an example of water pockets without bubbles is shown in Figure S1). These bubbles existed from the beginning of the observation, which indicates that they were not caused by the radiolysis of water. The encapsulated bubbles comprised air that was initially dissolved in the confined water. The high vacuum inside the TEM chamber expanded the two graphene layers and decreased the inner pressure, resulting in decreased air solubility and the generation of bubbles. The water-pocket diameters varied from 100 nm to 1 μ m, and each pocket had at the most one bubble that occupied 20–85% of its total area. Judging from the TEM images, the bubbles are in contact with both the

upper and lower graphene layers, as schematically shown in the inset of Figure 1.

Intense electron-beam irradiation causes radiolysis of water, which generates hydrogen molecules and results in the nucleation and the growth of nucleated nanobubbles.^{17–19} However, during our TEM observation, no radiolysis-induced bubble nucleation was observed. On the contrary, the existing bubbles often underwent sudden shrinkage. Because it is well known that graphene is weak against electron-beam irradiation,^{21–23} we assumed that the air inside the bubbles leaked from a newly generated hole in the graphene sheet; as a result, bubbles showed shrinkage. Thus, we investigated water pockets under different electron doses and acceleration voltages and identified the cause of graphene damage. We used two different types of electron guns: a thermionic electron gun and a field-emission (FE) gun. The electron dose rate of the thermionic electron source is lower by a factor of 100–1000 than that of the field-emission electron source.¹⁷ In this experiment, we used a JEM-2100Plus TEM with a LaB₆ filament thermionic electron gun and JEM-200F and JEM-200CF TEMs with FE guns. Each observation on one spot took at least 2 min. Damage to the graphene was judged by the bubble shrinkage and contrast change of the confined water, as shown in Figure S3.

Table 1 shows a correlation between the damage probability of the graphene and the electron-beam conditions. For the FE

Table 1. Damage Probabilities of Water Pockets under Different TEM Observation Conditions^a

electron gun	accelerating voltage (keV)	damaged	not damaged	damage probability (%)
FE gun	200	17	3	85.0
FE gun	60	5	6	45.5
thermionic gun	200	0	11	0.0

^aThe electron dose of the FE gun TEM is 100–1000 times higher than that of the thermionic gun.

gun, a lower damage probability was observed for the lower (60 keV) accelerating voltage. Furthermore, no damage to the graphene was found in a few minutes of observation with a 200 keV thermionic electron gun. Therefore, we could reduce the amount of damage to the water pockets by choosing a lower electron dose rate and lower acceleration voltage. This result is consistent with that of previous studies on electron-beam irradiation damage on single-layer graphene.²⁴

Next, we focused on the size of the water pockets and confined bubbles. In Figure 2, there was an overlap between the damaged (black symbols) and undamaged (white symbols) water pockets. Therefore, we concluded that there was no inter-relationship between the damage and the size of the water pockets. However, when water pockets did not have bubbles (symbols surrounded by the red circle in Figure 2), they were not damaged regardless of the electron-beam condition. This indicates that bubbles play an important role in the mechanism of water-pocket damage. A plausible explanation is that oxygen molecules in the bubbles chemically react with graphene under electron-beam irradiation and rapidly expand the damage.^{25,26} When there is no bubble, only electron sputtering causes damage to the graphene, which is much slower than the chemical reaction of oxygen and carbon.²⁴ This chemical etching effect of bubbles could be applied to new nano-

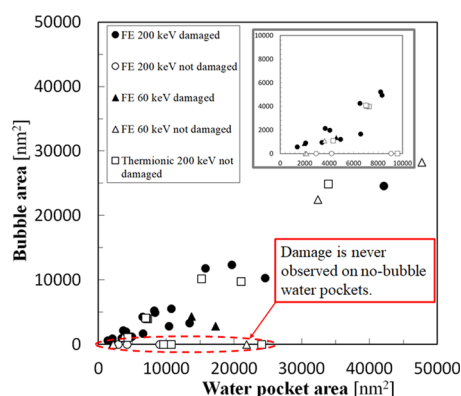


Figure 2. Relationship between the occurrence of water-pocket damage and the size of water pockets and the corresponding bubbles. Inset: enlarged view near the origin.

fabrication techniques of graphene, although this is outside the scope of this article.

To study the dynamic behavior, we intentionally caused damage to GLC water pockets using the FE electron gun operating at 200 keV and induced bubble movement. Figure 3 shows snapshot TEM images of the shrinkage, splitting, generation, and growth of bubbles in a water pocket (see Supporting movie S1 for the full movie). The initial bubble (Figure 3a) began to shrink shortly after entering the field of view of the microscope. Because two sections of the contact line (red lines in Figure 3c) experienced stronger pinning than other sections, the bubble became dumbbell-shaped^{17,27} and eventually broke into two bubbles (Figure 3f; labeled 1 and 2 in Figure 3k).

Immediately after splitting, the “tail” of bubble 1 retracted (Figure 3g,h) and the bubble became circular (Figure 3i), reducing its surface area, and bubble 3 appeared on the right side of bubble 1 (Figure 3g–i). Three seconds later (Figure 3j), bubbles 4 and 5 nucleated on the sides of bubble 3, owing

to the transport of gas molecules induced by the shrinking liquid/gas interface. The anisotropic shrinking of bubble 1 caused inner gas flow from left to right in the image in Figure 3. Figure 4 schematically illustrates the process as the gas

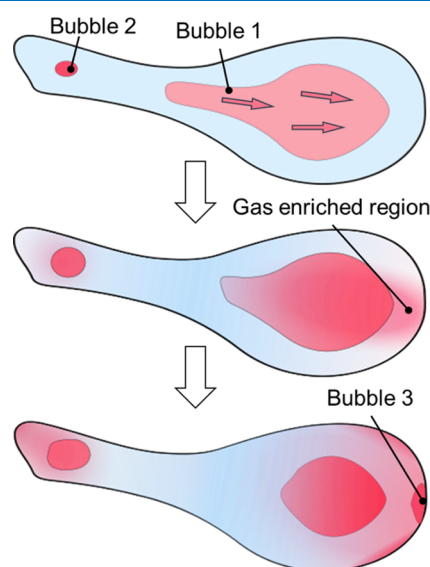


Figure 4. Schematic illustration of the bubble behavior and gas density variation in the water pocket.

molecules penetrate through the right-side interface of bubble 1 to create a gas-enriched region at the right side of the water pocket, resulting in the nucleation of bubble 3. Even after the nucleation of bubble 3, the gas supply from bubble 1 continued, which enabled the nucleation of bubbles 4 and 5. Because gas molecules near bubble 3 were consumed as it grew, nucleation points of bubbles 4 and 5 were a few tens of nanometers away from bubble 3. We note that bubbles 3–5 were generated at the edge of the water pocket, where they

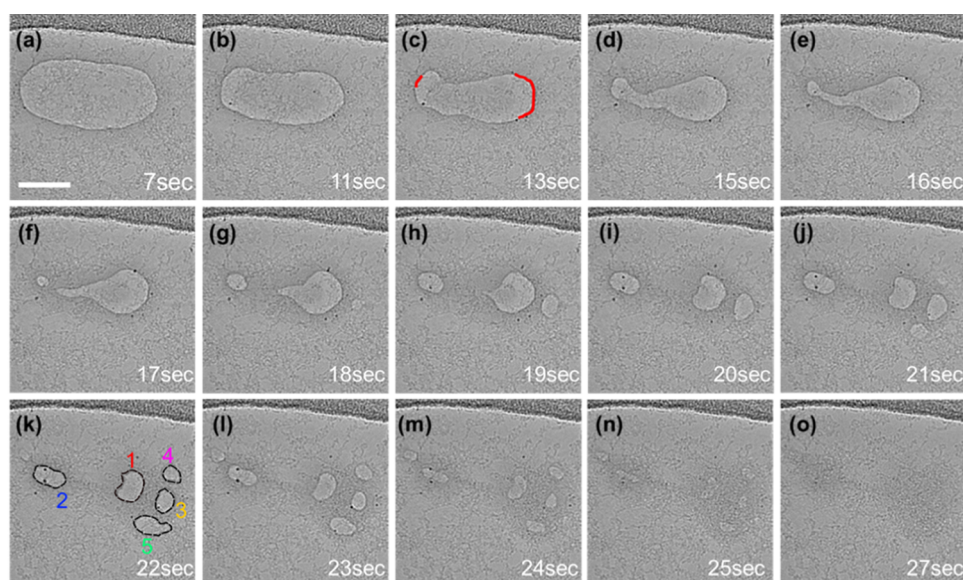


Figure 3. TEM images of a collapsing bubble as a function of time measured from when the bubble entered the TEM visual field (Supporting movie S1). The water pocket is the area with a darker contrast. The red lines in (c) indicate that the strongly pinned three-phase contact lines are stationary during collapse. Each bubble is numbered 1–5 in (k). All bubbles disappeared after 27 s. The timer started when the bubble entered the field of view. The scale bar indicates 50 nm.

could take advantage of thermodynamically favorable heterogeneous nucleation.

On the other hand, bubble 2 started growing from just after the splitting of the dumbbell-shaped bubble (Figure 3f). This sudden growth of bubble 2 was seemingly caused by the sudden change of Laplace pressure. Before the splitting (Figure 3a–e), the left part of the dumbbell-shaped bubble that became bubble 2 later experienced much larger Laplace pressure than after splitting because the radius of the dumbbell-shaped bubble was bigger than that of bubble 2. After the splitting, however, bubble 2 suddenly gained higher Laplace pressure, so it immediately started expanding to balance the pressure.

The nucleation of bubbles 3–5 indicates that an air-saturated area existed on the right side of the water pocket. When we consider bulk water, however, gas molecules leaking from bubble 1 to the water should spread uniformly through this water pocket. To investigate how rapidly the gas molecules diffuse in bulk water, the three-dimensional diffusion distance, x , in t seconds can be calculated as

$$x = \sqrt{6Dt} \quad (1)$$

where D is the diffusion coefficient, which is obtained by the Stokes–Einstein equation

$$D = \frac{k_B T}{6\pi\eta R} \quad (2)$$

where k_B is the Boltzmann constant, T is the absolute temperature of the solvent, η is the viscosity, and R is the radius of the solution. When we apply eqs 1 and 2 using the radius of a nitrogen molecule as a representative gas molecule ($R = 1.55 \times 10^{-10}$ m) and the viscosity of bulk water ($\eta = 9 \times 10^{-4}$ Pa·s) at $T = 300$ K, we obtain $D \approx 1.6 \times 10^{-9}$ m²·s^{−1}, signifying that a nitrogen molecule will move approximately 97 μm in 1 s. Considering the size of our water pocket, the leaked air from bubble 1 would immediately diffuse through the pocket, resulting in a uniform gas density. However, this theoretically estimated homogeneous gas density in the water pocket cannot explain the observed nucleation of bubbles 3–5. This indicates that the leaked gas did not spread uniformly through the water but moved in a nondiffusive manner.

Before discussing the mechanism of the nondiffusive behavior of gas molecules, the thickness of the water pocket should be determined. Unfortunately, no simple method exists to accurately measure the thickness of water pockets in GLCs. Thus, we roughly estimated the thickness from the Brownian motion of nanoparticles within the cells, which are likely to be the residue of the etched Cu/Ni film. Two Brownian particles 3 nm in diameter were tracked and their diffusion coefficients were calculated. Figure 5 shows TEM images of these two particles, which were found to move 2.7 and 4.6 nm, respectively, in 4 s, yielding diffusion coefficients of approximately 3.0×10^{-19} and 9.0×10^{-19} m²·s^{−1}, respectively, as calculated from eq 1. Small diffusion coefficient values such as these have been observed in several previous experiments.^{28–31} Lu et al. investigated the Brownian motion of 3–10-nm-diameter gold nanoparticles encapsulated in approximately 10–20-nm-thick water pockets. They concluded that the diffusion was damped by the high viscosity of the water near the solid wall, which is 9 orders of magnitude higher than that of bulk water.³¹ Because the size of the Brownian particles and diffusion coefficient in this previous work are similar to

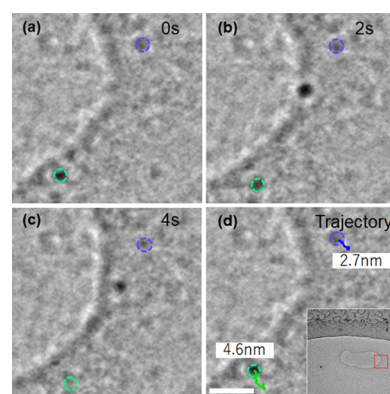


Figure 5. TEM images of two free-standing Brownian particles (a–c) as a function of time after observation and (d) their measured trajectories (colored lines). Particle movement was tracked for 4 s from the initial image given in Figure 3c. The scale bar is 5 nm. Inset: location in the TEM image at which these close-up images were obtained.

those of the present study, the thickness of the water pocket in this work may also be 10 nm or less, especially at the edge of the pocket.

Within thin water pockets, the confined water molecules interact strongly with the walls and form ordered-layer structures, called hydration layers, at the interface between the walls and water. Several reports have revealed that the thickness of hydration layers on graphene and highly oriented pyrolytic graphite substrates reaches 1–2 nm.^{32–35} Based on the thickness of the water pocket in the present study, we consider that hydration layers exist near both the upper and lower graphene sheets and that most water molecules are strongly linked with each other. This is consistent with the conclusions of a previous report on single-walled carbon nanotubes.¹² Consequently, collisions between gas and water molecules are suppressed, which leads to the nondiffusive behavior of the bubbles.

CONCLUSIONS

We observed the nanoscale bubble dynamics induced in GLCs under electron-beam irradiation. Water pockets with bubbles damaged the graphene at high electron doses, and the probability increased with increasing the accelerating voltage. By contrast, water pockets did not damage the graphene at low electron doses or when they did not contain any bubbles. We observed the dynamic behavior of the bubbles that induced GLC damage. We found that gas molecules in water films less than 10 nm thick exhibited nondiffusive behavior. We concluded that the nanoscale-confined water develops layered structures owing to the proximity to the graphene wall and that gas molecules are transported with a lower frequency of collision with water molecules. Understanding the bubble behavior in nanoscopically thin liquid films (including shrinkage, growth, deformation, and collapse) is important for expanding our knowledge of nanoporous materials. Therefore, on the basis of our study, the nondiffusive behavior of gas molecules should be considered for the design of nanofluidic devices. Future works with liquid cells made from other two-dimensional materials, such as boron nitride (BN) or molybdenum disulfide, will reveal the effect of the property of the solid on the behavior of bubbles at nanoscale solid/liquid interfaces.

■ ASSOCIATED CONTENT

Supporting Information

The Supporting Information is available free of charge at <https://pubs.acs.org/doi/10.1021/acsomega.0c01207>.

TEM image of water pockets (PDF)

TEM observation of bubble nucleation in the graphene liquidcell shown in Figure 3 (AVI)

■ AUTHOR INFORMATION

Corresponding Author

Koji Takahashi – Department of Aeronautics and Astronautics and International Institute for Carbon-Neutral Energy Research (WPI-I2CNER), Kyushu University, Fukuoka 819-0395, Japan; orcid.org/0000-0002-3552-9292; Phone: +81-92-802-3015; Email: takahashi@aero.kyushu-u.ac.jp

Authors

Sota Hirokawa – Department of Aeronautics and Astronautics, Kyushu University, Fukuoka 819-0395, Japan

Hideaki Teshima – Department of Aeronautics and Astronautics and International Institute for Carbon-Neutral Energy Research (WPI-I2CNER), Kyushu University, Fukuoka 819-0395, Japan

Pablo Solís-Fernández – Global Innovation Center, Kyushu University, Fukuoka 816-8580, Japan; orcid.org/0000-0003-1001-5874

Hiroki Ago – Global Innovation Center, Kyushu University, Fukuoka 816-8580, Japan; orcid.org/0000-0003-0908-5883

Yoko Tomo – Department of Mechanical Engineering, Kyushu University, Fukuoka 819-0395, Japan

Qin-Yi Li – Department of Aeronautics and Astronautics and International Institute for Carbon-Neutral Energy Research (WPI-I2CNER), Kyushu University, Fukuoka 819-0395, Japan; orcid.org/0000-0003-1388-7686

Complete contact information is available at:

<https://pubs.acs.org/doi/10.1021/acsomega.0c01207>

Notes

The authors declare no competing financial interest.

■ ACKNOWLEDGMENTS

This work was partially supported by the Japan Science and Technology Core Research for Evolutional Science and Technology (CREST) (Grant No. JPMJCR1811), Japan Society for the Promotion of Science Grants-in-Aid for Scientific Research (KAKENHI) (Grant Nos. JP17H03186 and JP19K23490), and a project commissioned by the New Energy and Industrial Technology Development Organization (NEDO), Japan. Some of the TEM observations were performed at the Ultramicroscopy Research Center, Kyushu University. We thank Prof. Masamichi Kohno and Tatsuya Ikuta for fruitful discussions and technical support.

■ REFERENCES

- (1) Whitby, M.; Quirke, N. Fluid Flow in Carbon Nanotubes and Nanopipes. *Nat. Nanotechnol.* **2007**, *2*, 87.
- (2) Zhang, X.; Liu, H.; Jiang, L. Wettability and Applications of Nanochannels. *Adv. Mater.* **2019**, *31*, No. 1804508.
- (3) Tomo, Y.; Askounis, A.; Ikuta, T.; Takata, Y.; Sefiane, K.; Takahashi, K. Superstable Ultrathin Water Film Confined in a Hydrophilized Carbon Nanotube. *Nano Lett.* **2018**, *18*, 1869–1874.

- (4) Li, Q. Y.; Matsushita, R.; Tomo, Y.; Ikuta, T.; Takahashi, K. Water Confined in Hydrophobic Cup-Stacked Carbon Nanotubes beyond Surface-Tension Dominance. *J. Phys. Chem. Lett.* **2019**, *10*, 3744–3749.

- (5) Hummer, G.; Rasaiah, J. C.; Noworyta, J. P. Water Conduction through the Hydrophobic Channel of a Carbon Nanotube. *Nature* **2001**, *414*, 188–190.

- (6) Majumder, M.; Chopra, N.; Andrews, R.; Hinds, B. J. Enhanced Flow in Carbon Nanotubes. *Nature* **2005**, *438*, 44.

- (7) Holt, J. K.; Park, H. G.; Wang, Y.; Stadermann, M.; Artyukhin, A. B.; Grigoropoulos, C. P.; Noy, A.; Bakajin, O. Fast Mass Transport Through Sub-2-Nanometer Carbon Nanotubes. *Science* **2006**, *312*, 1034–1037.

- (8) Joseph, S.; Aluru, N. R. Why Are Carbon Nanotubes Fast Transporters of Water? *Nano Lett.* **2008**, *8*, 452–458.

- (9) Secchi, E.; Marbach, S.; Niguès, A.; Stein, D.; Siria, A.; Bocquet, L. Massive Radius-Dependent Flow Slippage in Carbon Nanotubes. *Nature* **2016**, *537*, 210–213.

- (10) Whitby, M.; Cagnon, L.; Thanou, M.; Quirke, N. Enhanced Fluid Flow through Nanoscale Carbon Pipes. *Nano Lett.* **2008**, *8*, 2632–2637.

- (11) Chaban, V. V.; Prezhdov, O. V. Water Boiling inside Carbon Nanotubes: Toward Efficient Drug Release. *ACS Nano* **2011**, *5*, 5647–5655.

- (12) Agrawal, K. V.; Shimizu, S.; Drahushuk, L. W.; Kilcoyne, D.; Strano, M. S. Observation of Extreme Phase Transition Temperatures of Water Confined inside Isolated Carbon Nanotubes. *Nat. Nanotechnol.* **2017**, *12*, 267–273.

- (13) Koga, K.; Gao, G. T.; Tanaka, H.; Zeng, X. C. Formation of Ordered Ice Nanotubes inside Carbon Nanotubes. *Nature* **2001**, *412*, 802–805.

- (14) Bai, J.; Wang, J.; Zeng, X. C. Multiwalled Ice Helices and Ice Nanotubes. *Proc. Natl. Acad. Sci. U.S.A.* **2006**, *103*, 19664–19667.

- (15) Mashl, R. J.; Joseph, S.; Aluru, N. R.; Jakobsson, E. Anomalous Immobilized Water: A New Water Phase Induced by Confinement in Nanotubes. *Nano Lett.* **2003**, *3*, 589–592.

- (16) Tomo, Y.; Takahashi, K.; Nishiyama, T.; Ikuta, T.; Takata, Y. Nanobubble Nucleation Studied Using Fresnel Fringes in Liquid Cell Electron Microscopy. *Int. J. Heat Mass Transfer* **2017**, *108*, 1460–1465.

- (17) Shin, D.; Park, J. B.; Kim, Y. J.; Kim, S. J.; Kang, J. H.; Lee, B.; Cho, S. P.; Hong, B. H.; Novoselov, K. S. Growth Dynamics and Gas Transport Mechanism of Nanobubbles in Graphene Liquid Cells. *Nat. Commun.* **2015**, *6*, No. 6068.

- (18) Yang, J.; Alam, S. B.; Yu, L.; Chan, E.; Zheng, H. Dynamic Behavior of Nanoscale Liquids in Graphene Liquid Cells Revealed by in Situ Transmission Electron Microscopy. *Micron* **2019**, *116*, 22–29.

- (19) Kim, Qh.; Shin, D.; Park, J.; Weitz, D. A.; Jhe, W. Initial Growth Dynamics of 10 Nm Nanobubbles in the Graphene Liquid Cell. *Appl. Nanosci.* **2018**, *1*–7.

- (20) Takesaki, Y.; Kawahara, K.; Hibino, H.; Okada, S.; Tsuji, M.; Ago, H. Highly Uniform Bilayer Graphene on Epitaxial Cu-Ni(111) Alloy. *Chem. Mater.* **2016**, *28*, 4583–4592.

- (21) Wang, W. L.; Santos, E. J. G.; Jiang, B.; Cubuk, E. D.; Ophus, C.; Centeno, A.; Pesquera, A.; Zurutuza, A.; Ciston, J.; Westervelt, R.; et al. Direct Observation of a Long-Lived Single-Atom Catalyst Chiseling Atomic Structures in Graphene. *Nano Lett.* **2014**, *14*, 450–455.

- (22) Girit, ÇÖ.; Meyer, J. C.; Erni, R.; Rossell, M. D.; Kisielowski, C.; Yang, L.; Park, C. H.; Crommie, M. F.; Cohen, M. L.; Louie, S. G.; et al. Graphene at the Edge: Stability and Dynamics. *Science* **2009**, *323*, 1705–1708.

- (23) Kotakoski, J.; Santos-Cottin, D.; Krashennnikov, A. V. Stability of Graphene Edges under Electron Beam: Equilibrium Energetics versus Dynamic Effects. *ACS Nano* **2012**, *6*, 671–676.

- (24) Meyer, J. C.; Eder, F.; Kurasch, S.; Skakalova, V.; Kotakoski, J.; Park, H. J.; Roth, S.; Chuvilin, A.; Eychen, S.; Benner, G.; et al. Accurate Measurement of Electron Beam Induced Displacement

Cross Sections for Single-Layer Graphene. *Phys. Rev. Lett.* **2012**, *108*, 1–6.

(25) Mølhave, K.; Gudnason, S. B.; Pedersen, A. T.; Clausen, C. H.; Horsewell, A.; Bøggild, P. Electron Irradiation-Induced Destruction of Carbon Nanotubes in Electron Microscopes. *Ultramicroscopy* **2007**, *108*, 52–57.

(26) Sommer, B.; Sonntag, J.; Ganczarczyk, A.; Braam, D.; Prinz, G.; Lorke, A.; Geller, M. Electron-Beam Induced Nano-Etching of Suspended Graphene. *Sci. Rep.* **2015**, *5*, No. 7781.

(27) Teshima, H.; Nishiyama, T.; Takahashi, K.; Teshima, H.; Nishiyama, T.; Takahashi, K. Nanoscale Pinning Effect Evaluated from Deformed Nanobubbles Nanoscale Pinning Effect Evaluated from Deformed Nanobubbles **2017**, *146*, 014708. DOI: 10.1063/1.4973385.

(28) Zheng, H.; Claridge, S. A.; Minor, A. M.; Alivisatos, A. P.; Dahmen, U. Nanocrystal Diffusion in a Liquid Thin Film Observed by in Situ Transmission Electron Microscopy. *Nano Lett.* **2009**, *9*, 2460–2465.

(29) Grogan, J. M.; Rotkina, L.; Bau, H. H. In Situ Liquid-Cell Electron Microscopy of Colloid Aggregation and Growth Dynamics. *Phys. Rev. E: Stat., Nonlinear, Soft Matter Phys.* **2011**, *83*, No. 061405.

(30) Verch, A.; Pfaff, M.; De Jonge, N. Exceptionally Slow Movement of Gold Nanoparticles at a Solid/Liquid Interface Investigated by Scanning Transmission Electron Microscopy. *Langmuir* **2015**, *31*, 6956–6964.

(31) Lu, J.; Aabdin, Z.; Loh, N. D.; Bhattacharya, D.; Mirsaidov, U. Nanoparticle Dynamics in a Nanodroplet. *Nano Lett.* **2014**, *14*, 2111–2115.

(32) Schlesinger, I.; Sivan, U. Three-Dimensional Characterization of Layers of Condensed Gas Molecules Forming Universally on Hydrophobic Surfaces. *J. Am. Chem. Soc.* **2018**, *140*, 10473–10481.

(33) Yang, C. W.; Miyazawa, K.; Fukuma, T.; Miyata, K.; Hwang, I. S. Direct Comparison between Subnanometer Hydration Structures on Hydrophilic and Hydrophobic Surfaces via Three-Dimensional Scanning Force Microscopy. *Phys. Chem. Chem. Phys.* **2018**, *20*, 23522–23527.

(34) Utsunomiya, T.; Yokota, Y.; Enoki, T.; Fukui, K. I. Potential-Dependent Hydration Structures at Aqueous Solution/Graphite Interfaces by Electrochemical Frequency Modulation Atomic Force Microscopy. *Chem. Commun.* **2014**, *50*, 15537–15540.

(35) Suzuki, K.; Oyabu, N.; Kobayashi, K.; Matsushige, K.; Yamada, H. Atomic-Resolution Imaging of Graphite-Water Interface by Frequency Modulation Atomic Force Microscopy. *Appl. Phys. Express* **2011**, *4*, No. 125102.